Satellite-based quantum steering with continuous variables

Qianqian Liu,[1,*] Shu-Min Wu,[2,†] Cuihong Wen,[3] and Jieci Wang[3,‡]

[1]*Department of Physics, Xiangtan University, Xiangtan 411105, Hunan Province, China*
[2]*Department of Physics, Liaoning Normal University, Dalian 116029, China*
[3]*Department of Physics, Key Laboratory of Low Dimensional Quantum Structures and Quantum Control of Ministry of Education, Hunan Normal University, Changsha 410081, China*

(Received 20 November 2025; accepted 9 June 2026; published 26 June 2026)

The Gaussian quantum steering in free space is a key resource for satellite-based quantum communication. In this work, we model the free space transmission of Gaussian states as a fading and noisy quantum channel, incorporating key loss mechanisms including diffraction, atmospheric attenuation, turbulence, and receiver-side background photons. Our study encompasses a broad range of practical conditions, including uplink and downlink transmission, and daytime and nighttime operation. We show that Gaussian steerability decreases monotonically with satellite altitude, transitioning from two-way to one-way steering and ultimately to nonsteerability. Furthermore, we find that the nighttime downlink channel experiences the lowest overall loss and exhibits the greatest robustness, thereby providing the most favorable conditions for achieving Gaussian quantum steerability. Our results quantitatively characterize channel-induced steering asymmetry and provide guidelines for optimizing continuous-variable satellite quantum communication.

DOI: 10.1103/br47-p9rt

I. INTRODUCTION

The realization of long-distance quantum communication is a fundamental milestone toward the development of global quantum networks [1–3]. In recent years, substantial effort has focused on studying quantum correlations and quantum key distribution between ground-based stations and low-Earth-orbit satellites, which form essential links for interconnecting terrestrial quantum networks on a global scale [4–7]. Quantum steering, a distinct form of quantum correlation, characterizes the ability of local measurements performed on one subsystem to remotely influence the conditional states of another spatially separated subsystem [8–10]. It occupies an intermediate position in the hierarchy of quantum correlations, lying between entanglement and Bell nonlocality. Operationally, steering asks whether one party can demonstrate that the other party's conditional states, inferred from measurement outcomes, cannot be explained by any local hidden-state model. In this sense, steering captures an intrinsically directional form of quantum correlation. The directional characteristics of quantum steering are of vital importance for applications ranging from quantum random number generation to secure information transfer across quantum networks [11–13]. A notable feature of quantum steering is its intrinsic asymmetry—Alice may be able to steer Bob, while the converse does not necessarily hold. Steerability in a given direction constitutes the operational resource for one-sided device-independent quantum key distribution, as it enables information-theoretic security even when one party's device is untrusted [14–20].

On the other hand, free space quantum channels are inherently lossy and noisy. The impact of atmospheric turbulence on classical optical signals has been extensively characterized [21,22], and recent studies have extended such investigations to quantum atmospheric channels, demonstrating that the nonclassical properties of quantum states can be preserved under realistic conditions [23,24]. In such channels, optical signals propagating through the atmosphere are significantly affected by diffraction, atmospheric extinction, and turbulence-induced fluctuations. In addition, the received signal is inevitably contaminated by environmental background photons collected at the detection stage. These effects collectively give rise to fading and noisy quantum channels, where the transmittance varies randomly due to deterministic attenuation and random perturbations [6,24–26]. Given these accurate channel models, a detailed assessment of quantum state propagation across different operational conditions (uplink/downlink and daytime/nighttime operation) is vital for understanding how such environments modify the symmetry properties of Gaussian quantum steering. This evaluation is key to determining the feasibility and enhancing the performance of satellite-based quantum communication systems.

In this study, we assume that the ground and satellite observers initially share a two-mode squeezed vacuum state for implementing the quantum steering protocol. During free space propagation, the optical field at wavelength $\lambda = 800\,\mathrm{nm}$ undergoes diffraction and atmospheric attenuation, while the receiver-side background noise further degrades the received signal quality. In addition, atmospheric turbulence gives rise to beam wandering and beam broadening. Collectively, these effects result in an instantaneous lossy fading and noisy

*Contact author: qianqianliu@xtu.edu.cn
†Contact author: smwu@lnnu.edu.cn
‡Contact author: jcwang@hunnu.edu.cn

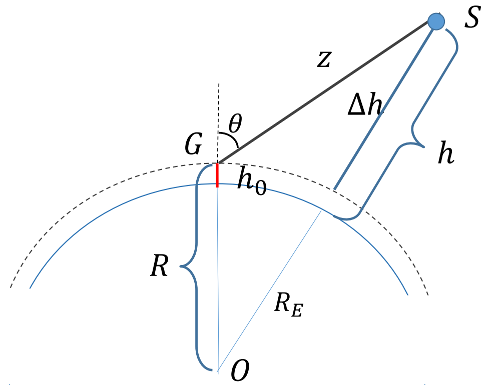

FIG. 1. Basic geometry for satellite communications. A satellite (S) at altitude h is observed from a ground station (G) at the zenith angle θ, corresponding to the slant propagation distance z.

channel between the ground station and the satellite. Using the covariance matrix formalism for Gaussian states, we evaluate the steerability under both uplink and downlink configurations. The results show the Gaussian steerability consistently decreases with increasing satellite altitude, transitioning from two-way to one-way steering and eventually vanishing. Moreover, we find that nighttime downlink operation offers the most favorable conditions for maintaining free space Gaussian quantum steerability. By examining the influence of squeezing parameters and receiver configurations on Gaussian quantum steering, we gain deeper insight into how to mitigate the loss mechanisms of optical signals during propagation in free space.

This paper is structured as follows. Section II details the free space propagation of optical signals between the ground station and the satellite, with an emphasis on incorporating the various error sources that influence signal transmission. Section III provides a brief introduction to the definition and quantification of Gaussian steering. In Sec. IV, we investigate the distribution characteristics of Gaussian steerability in free space optical communication systems. Finally, the conclusions are drawn in Sec. V.

II. THEORETICAL FRAMEWORK

In this study, we consider communication between a ground station at height h_0 and a satellite in orbit at a radius of $R_0 = h + R_E$, where the satellite's height relative to Earth's surface is given by h, with R_E representing the Earth's radius (see Fig. 1). When observed from the ground station at the zenith angle θ, the effective altitude of the satellite is denoted by [4,5]

$$z = \sqrt{(\Delta h)^2 + 2\Delta h R + R^2\cos^2\theta} - R\cos\theta, \tag{1}$$

where

$$\Delta h = h - h_0 = \sqrt{R^2 + z^2 + 2zR\cos\theta} - R, \quad R = R_E + h_0, \tag{2}$$

and we specifically focus on the case of zenith communication, corresponding to $\theta = 0$. Hereafter, the ground station is assumed to be located at sea level ($h_0 = 0$).

We examine the propagation of optical signals from the ground station to the satellite through free space, considering the various environmental factors that affect this transmission. Each of these physical processes is modeled as an independent attenuation channel, characterized by the transmittance parameter τ_i. The effect of each channel is described using a beam-splitter model [27–30]. The optical mode $\hat{a}$ can be decomposed into the signal mode $\hat{a}$ and the thermal mode $\hat{a}_{\rm th}$:

$$\begin{aligned} \hat{a} &\longrightarrow \sqrt{\tau_i}\hat{a} + \sqrt{1-\tau_i}\hat{a}_{\rm th}, \\ \hat{a}_{\rm th} &\longrightarrow \sqrt{\tau_i}\hat{a}_{\rm th} - \sqrt{1-\tau_i}\hat{a}. \end{aligned} \tag{3}$$

The propagation of optical signals in free space is a combined effect of different loss mechanisms, and the total loss rate is $\tau = \prod_{i=1}^{N} \tau_i$ [4–6,25].

A. Diffraction

In this subsection, we analyze the influence of diffraction on the free space propagation of optical signals. The optical field is modeled as a quasimonochromatic bosonic mode, represented by a Gaussian beam with the wavelength λ, the initial waist ω_0, and the wave-front curvature radius R_0. In the collimated case, the curvature radius is taken as $R_0 \to \infty$. The beam is prepared by the transmitter (whose aperture is sufficiently larger than ω_0) and directed toward the receiver, whose aperture is circular with the radius a_R. The Rayleigh range is given by $z_R = \pi\omega_0^2/\lambda$. The far-field condition is satisfied when the transmission distance z fulfills $z \gg z_R$.

During propagation, the beam radius evolves as

$$\omega_z^2 = \omega_0^2\left[1 + \left(\frac{z}{z_R}\right)^2\right], \tag{4}$$

which explicitly quantifies the diffraction-induced spreading of the Gaussian mode as a function of propagation distance. The transmissivity induced by diffraction is given by [31]

$$\tau_{\rm diff} = 1 - e^{-2(a_R/\omega_z)^2}. \tag{5}$$

B. Atmospheric attenuation

The transmissivity of an optical signal affected by atmospheric attenuation at a fixed altitude is denoted as [5,6]

$$\tau_{\rm atm} = \exp[-\alpha_0 z e^{-h/\tilde{h}}]. \tag{6}$$

The attenuation is quantified through the extinction coefficient $\alpha_0 = N_0\sigma$, where N_0 represents the particle density, and $\sigma = \sigma_{\rm abs} + \sigma_{\rm sca}$ is the total cross section, accounting for both absorption and scattering processes. A typical atmospheric scale height is taken as $\tilde{h} = 6600$ m [4]. At sea level, for a Gaussian beam with a wavelength of $\lambda = 800$ nm, the extinction factor is estimated as $\alpha_0 = 5 \times 10^{-6}$ m^{-1}. When the satellite altitude is treated as a variable, the corresponding transmissivity of the optical link from the ground to the satellite, under the influence of atmospheric attenuation, is denoted by

$$\tau_{\rm atm} = e^{-\alpha_0 \int_0^{z(h,\theta)} {\rm d}y e^{-h(y,\theta)/\tilde{h}}}. \tag{7}$$

C. Detector efficiency and thermal background

In atmospheric free space optical communication, the efficiency of the detector plays a significant role in the overall transmissivity of the channel. An ideal detector has efficiency $\tau_{\text{eff}} = 1$, while for a nonideal detector $\tau_{\text{eff}} < 1$. In addition to detecting signal photons, the detector also captures thermal radiation from the atmosphere, modeled by the thermal mode operator $\hat{a}_{\text{th}}$. The average number of thermal photons detected is given by $\tau_{\text{eff}} n$, where n represents the mean number of thermal photons from the background environment. We assume that the number of effective thermal photons that the signal path receives corresponds to the number of thermal photons the detector can capture. For quantitative analysis, we define the parameters [5]

$$\begin{aligned} \Gamma_R &= \Delta\lambda \Delta t \Omega_{\text{fov}} a_R^2, \\ N_{\text{BB}} &= 2c\lambda^{-4}[e^{h_p c/(\lambda k_B T)} - 1]^{-1}, \\ n &= \Gamma_R N_{\text{BB}}, \end{aligned} \tag{8}$$

where Γ_R is the photon collection efficiency, Δt and $\Delta\lambda$ are the detection time and spectral filter, respectively, a_R and Ω_{fov} are the aperture radius and the field of view of the receiver, and N_{BB} represents the thermal photon number derived from the black-body radiation formula, expressed in units of Γ_R^{-1}. In addition, c represents the speed of light, h_p is Planck's constant, κ_B denotes Boltzmann's constant, T is the temperature, and n is the mean thermal photon number.

We take $\Delta t = 10$ ns and $\Delta\lambda = 1$ nm for the detector, and $\Omega_{\text{fov}} = 10^{-10}$ sr and $a_R = 40$ cm for the receiving telescope [5]. Under these conditions, the mean thermal photon number is calculated for both downlink and uplink configurations. For the downlink channel, the average thermal photon number is $n_{\text{day}}^{\text{down}} = 0.30$ during the daytime and $n_{\text{night}}^{\text{down}} = 3.40 \times 10^{-6}$ at night. For the uplink channel, the corresponding values are $n_{\text{day}}^{\text{up}} = 0.22$ and $n_{\text{night}}^{\text{up}} = 5.43 \times 10^{-7}$ [5,32,33].

D. Turbulence

In this section, we examine the impact of weak atmospheric turbulence on the propagation of optical signals in free space, which is typically representative of high-elevation-angle satellite links, and in this work we focus on the zenith communication configuration. Under weak turbulence, the received beam profile is jointly determined by diffraction and turbulence-induced fluctuations over different spatial scales [21,22]. The short-term beam width characterizes the instantaneous beam spot including diffraction and turbulence-induced spreading, while the long-term beam width additionally incorporates centroid fluctuations associated with beam wandering. In this sense, the long-term beam profile should be understood as the net statistical result of diffraction together with the combined effects of small-scale and large-scale turbulent eddies. Correspondingly, the beam centroid exhibits random displacement around the receiver center, which can be quantified by a beam-wandering variance σ_{TB}^2. Additional pointing errors contribute a variance of $\sigma_{\text{P}}^2 \simeq (10^{-6}z)^2$, yielding a total centroid variance of $\sigma^2 = \sigma_{\text{TB}}^2 + \sigma_{\text{P}}^2$.

We explicitly derive the parameters ω_{st} and σ_{TB}^2 based on turbulence models suitable for satellite communications. The propagation channel can be characterized by the spherical wave coherence radius, which for the uplink configuration is given by [21,22]

$$\rho_0 = \left[1.46k^2 \int_0^z \mathrm{d}\xi \left(1 - \frac{\xi}{z}\right)^{\frac{5}{3}} C_n^2[h(\xi,\theta)]\right]^{\frac{-3}{5}}. \tag{9}$$

For the downlink configuration, the corresponding expression is obtained by replacing the propagation variable according to $\xi \to z - \xi$. For a beam with a wave number of $k = 2\pi/\lambda$ propagating over a distance z, the spherical wave coherence radius is expressed as

$$\rho_0 = \left(0.548k^2 C_n^2 z\right)^{-3/5}, \tag{10}$$

where C_n^2 is the refractive index structure parameter, which measures the strength of fluctuations in the refractive index induced by spatial variations of temperature and pressure, and is typically modeled using the Hufnagel-Valley turbulence model [34,35]:

$$\begin{aligned} C_n^2 =& 5.94 \times 10^{-53}\left(\frac{v}{27}\right)^2 h^{10} e^{-h/1000} \\ &+ 2.7 \times 10^{-16} e^{-h/1500} + A e^{-h/100}. \end{aligned} \tag{11}$$

We take the wind speed $v = 21$ m/s, and $A_{\text{day(night)}} = 2.75(1.7) \times 10^{-14}$ m$^{-2/3}$ for daytime (nighttime). In this regime, the long-term beam waist can be approximated by [6]

$$\omega_{\text{lt}}^2 \simeq \omega_z^2 + 2\left(\frac{\lambda z}{\pi \rho_0}\right)^2. \tag{12}$$

Beam broadening is caused by the interaction of the beam with vortices smaller than the beam waist and acts on a fast timescale, which will replace the beam waist of the Gaussian beam from τ_z to τ_{st}:

$$\tau_{\text{st}} = 1 - e^{-2(a_R/\omega_{\text{st}})^2}. \tag{13}$$

Here, we can write

$$\omega_{\text{st}}^2 \simeq \omega_z^2 + 2\left(\frac{\lambda z}{\pi \rho_0}\right)^2 (1-\phi)^2, \quad \phi = 0.33(\rho_0/\omega_0)^{1/3}, \tag{14}$$

where ω_0 plays the role of the effective transverse scale of the transmitted Gaussian beam. In the weak turbulence regime, where $\phi \ll 1$, we can approximate $(1-\phi)^2 \approx 1 - 0.66(\rho_0/\omega_0)^{1/3}$ [25,26,36]. The large-scale turbulence variance is related to the corresponding short-term turbulence parameters through

$$\sigma_{\text{TB}}^2 = \omega_{\text{lt}}^2 - \omega_{\text{st}}^2 \approx \frac{0.1337\lambda^2 z^2}{\omega_0^{1/3}\rho_0^{5/3}}. \tag{15}$$

When the communication system operates within the near-zenith angle and with moderately sized receiver apertures, the impact of atmospheric turbulence on the downlink process can be neglected [5]. In this regime, the atmospheric path is shortest, and the receiver aperture captures most of the optical beam. Therefore, the long-term beam width can be accurately approximated as $w_{\text{lt}} \simeq w_{\text{st}} \simeq w_z$, with σ_{TB}^2 effectively set to 0.

We consider the parameter q as the instantaneous displacement between the beam centroid and its original center, also known as deflection. The Gaussian random walk around the receiver center induces a Weibull distribution for the deflection q, which is expressed by a zero-mean density function,

$$P_{\rm WB}(q) = \frac{q}{\sigma^2} e^{-\frac{q^2}{2\sigma^2}}. \tag{16}$$

For each instantaneous deflection q, the corresponding transmissivity $\tau(q) \leqslant \tau_{\max}$ happens with a probability $P(\tau)$. Each realization of q therefore corresponds to a total transmissivity,

$$\tau(q) = \tau_{\rm st}(q)\tau_{\rm atm}\tau_{\rm eff}. \tag{17}$$

The maximum transmissivity is $\tau_{\max} = \tau_{\rm st}(q = 0)\tau_{\rm atm}\tau_{\rm eff}$. The probability distribution over q induces then another probability distribution over τ [5,24],

$$P(\tau) = \frac{q_0^2}{\gamma\sigma^2\tau}\left(\ln\frac{\tau_{\max}}{\tau}\right)^{\frac{2}{\gamma}-1}\exp\left[-\frac{q_0^2}{2\sigma^2}\left(\ln\frac{\tau_{\max}}{\tau}\right)^{\frac{2}{\gamma}}\right], \tag{18}$$

where we have defined [6]

$$\begin{aligned} q_0 &= a_R\left[\ln\left(\frac{2\tau_{\rm st}}{1-\Lambda_0\left(\tau_{\rm st}^{\rm far}\right)}\right)\right]^{-1/\gamma}, \\ \gamma &= \frac{4\tau_{\rm st}^{\rm far}\Lambda_1\left(\tau_{\rm st}^{\rm far}\right)}{1-\Lambda_0\left(\tau_{\rm st}^{\rm far}\right)}\left[\ln\left(\frac{2\tau_{\rm st}}{1-\Lambda_0\left(\tau_{\rm st}^{\rm far}\right)}\right)\right]^{-1}, \\ \tau_{\rm st}^{\rm far} &= \frac{2a_R^2}{\omega_{\rm st}^2}, \quad \Lambda_n(x) = e^{-2x}I_n(2x). \end{aligned} \tag{19}$$

III. MEASUREMENT OF QUANTUM STEERABILITY FOR CONTINUOUS VARIABLES

In this section we quantify Gaussian steering, i.e., steerability under the restriction to Gaussian measurements on the steering party. Therefore, when the Gaussian steering measure vanishes, this indicates the absence of steerability within the Gaussian measurement framework, but does not exclude the possibility that steering could be revealed using non-Gaussian measurements. We consider a quantum steering measurement of the two-body Gaussian state σ_{AB} of the $(n + m)$ mode system [37]. The first moment of this state is 0 and its covariance matrix is expressed in normalized block form as

$$\sigma_{AB} = \begin{pmatrix} A & C \\ C & B \end{pmatrix}, \tag{20}$$

where A represents the $2n \times 2n$ covariance submatrix for subsystem Alice, and B is the $2m \times 2m$ covariance submatrix for subsystem Bob. For σ_{AB} to describe a physical Gaussian state, its covariance matrix must satisfy the uncertainty relation (the so-called bona fide condition), i.e.,

$$\sigma_{AB} + i(\Omega_A \oplus \Omega_B) \geqslant 0, \quad \Omega_A = \bigoplus_{k=1}^{n_A} J, \quad \Omega_B = \bigoplus_{k=1}^{n_B} J, \tag{21}$$

where $J = \left(\begin{smallmatrix} 0 & 1 \\ -1 & 0 \end{smallmatrix}\right)$ is the standard single-mode symplectic form. If Alice's measurement R_A yields a result r_A, the conditional state $\rho^{r_A|R_A}$ is also a Gaussian state, and its covariance matrix remains independent of the specific measurement outcome from Alice. The existence of Gaussian steering from Alice to Bob is equivalent to the violation of the steering inequality [9]:

$$\sigma_{AB} + i(0_A \oplus \Omega_B) \geqslant 0. \tag{22}$$

This violation serves as both a necessary and sufficient condition for demonstrating quantum steering from Alice to Bob in the state σ_{AB}. When Bob's subsystem is single mode, the steerability measure simplifies to the closed form [10]

$$\begin{aligned} \mathcal{G}^{A\to B}(\sigma_{AB}) &= \max\left\{0, \frac{1}{2}\ln\frac{\det A}{\det\sigma_{AB}}\right\}, \\ &= \max\{0, \mathcal{S}(A) - \mathcal{S}(\sigma_{AB}). \end{aligned} \tag{23}$$

For Gaussian states, there is a one-to-one correspondence between the quantum state ρ and its covariance matrix σ. $\mathcal{S}(\rho) = \frac{1}{2}\ln\det\sigma$ is the von Neumann entropy of a Gaussian state ρ [38]. Similarly, Gaussian steering in the opposite direction $(B \to A)$ is obtained by swapping the roles of subsystems A and B, leading to an expression structurally similar to Eq. (23). This directional dependence highlights the inherent asymmetry of Gaussian quantum steering: while Alice can steer Bob, the converse $B \to A$ is not necessarily possible.

IV. THE INFLUENCE OF SATELLITE QUANTUM COMMUNICATIONS ON QUANTUM STEERABILITY

The initial state of the modes is prepared by the two-mode squeezed vacuum state with the squeezing parameter s, which is described by the covariance matrix [39]

$$\sigma_{AB} = \begin{pmatrix} \cosh(2s)I_2 & \sinh(2s)\sigma_z \\ \sinh(2s)\sigma_z & \cosh(2s)I_2 \end{pmatrix}, \tag{24}$$

where $I_2 = {\rm diag}(1, 1)$ and $\sigma_z = {\rm diag}(1, -1)$. In the uplink configuration, mode A remains at the ground station, while only mode B is transmitted through the turbulent atmosphere to the satellite receiver. The transmission through the atmosphere can be modeled as an attenuation channel with transmissivity τ, which mixes the mode of the quantum state with a thermal mode from the environment. The thermal mode is described by a Gaussian state with its covariance matrix:

$$E_T = mI_2, \quad m = 1 + 2\tau_{\rm eff}n. \tag{25}$$

Here, $\tau_{\rm eff}$ represents the effective detection efficiency, and $n \in \{n_{\rm day}^{\rm down}, n_{\rm day}^{\rm up}, n_{\rm night}^{\rm down}, n_{\rm night}^{\rm up}\}$ indicates the mean thermal photon number under different link conditions.

The covariance matrix of the joint state after propagation is denoted by

$$\begin{aligned} \sigma'_{ABT} = {}&[I_A \oplus S_{B,T}][\sigma_{AB} \oplus E_T] \\ &[I_A \oplus S_{B,T}]^\top. \end{aligned} \tag{26}$$

The transformation in phase space, as shown in Eq. (3) can be expressed by a symplectic operator,

$$S_{B,T} = \begin{pmatrix} \sqrt{\tau}I_2 & \sqrt{1-\tau}I_2 \\ -\sqrt{1-\tau}I_2 & \sqrt{\tau}I_2 \end{pmatrix}. \tag{27}$$

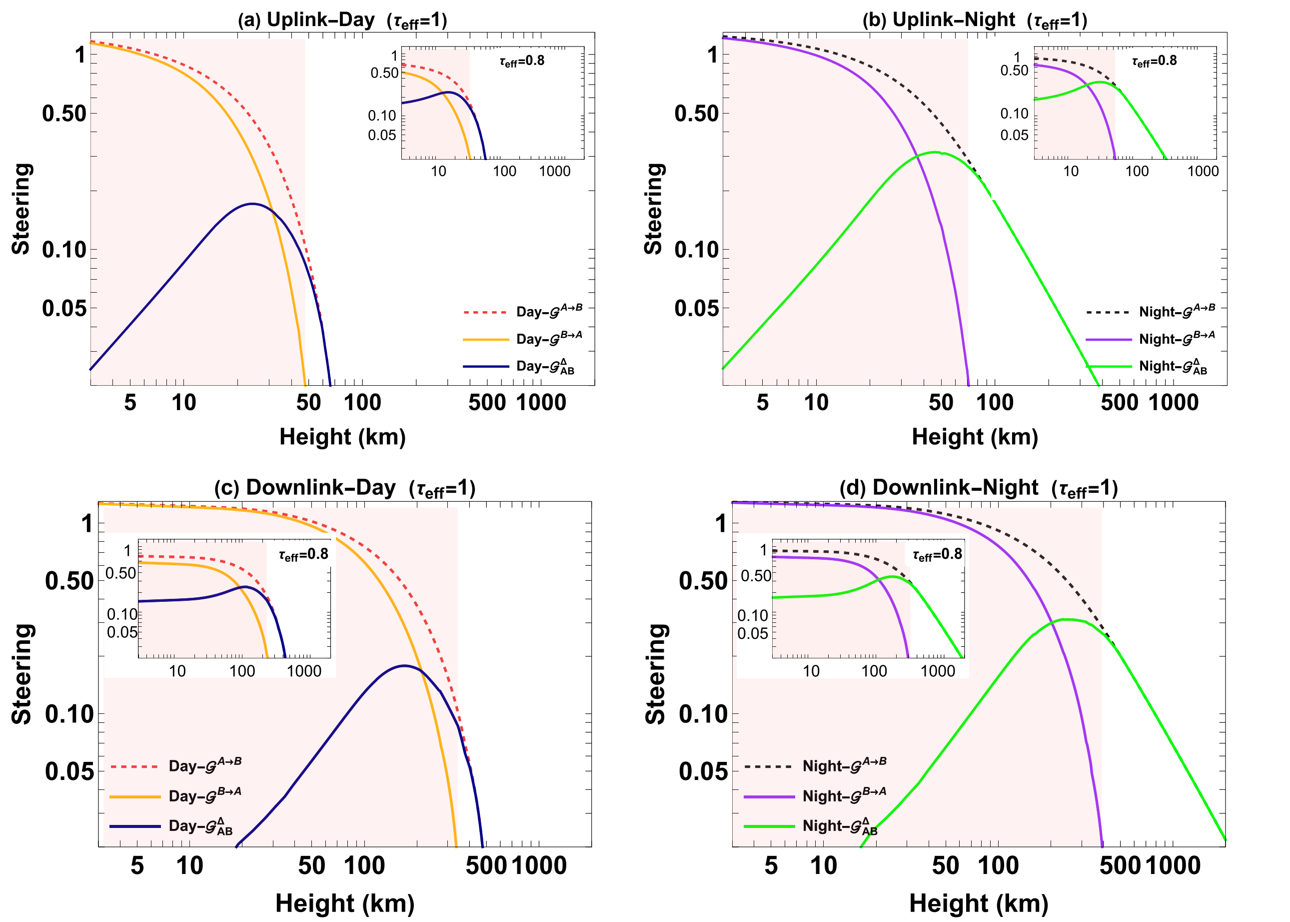

FIG. 2. Gaussian quantum steering for uplink and downlink transmissions between a ground station and a satellite. The main plot shows an ideal detector with $\tau_{\text{eff}} = 1$, while the inset illustrates a realistic detector with $\tau_{\text{eff}} = 0.8$. Transmission is modeled using a two-mode squeezed vacuum state propagating through free space, subject to diffraction, atmospheric extinction, turbulence, and receiver-side background photons. Parameters are as follows: wavelength $\lambda = 800$ nm, squeezing $s = 1$, beam waist $\omega_0 = 20$ cm, and receiver aperture $a_R = 40$ cm. The pale red shaded region marks the regime where two-way Gaussian steering is possible. Gaussian nonsteerability in the high-loss regime reflects the limitations of Gaussian measurements, rather than a fundamental impossibility of satellite-based continuous variable steering.

Taking the trace over the thermal mode, we obtain the bipartite system for Alice and Bob:

$$\sigma'_{AB} = \begin{pmatrix} \cosh(2s)I_2 & \sqrt{\tau}\sinh(2s)\sigma_z \\ \sqrt{\tau}\sinh(2s)\sigma_z & [\tau\cosh(2s) + (1-\tau)m]I_2 \end{pmatrix}. \tag{28}$$

The explicit derivation of the output covariance matrix is given in Appendix A. Employing Eq. (23), we obtain an analytic expression of the quantum steerability from Alice to Bob,

$$\mathcal{G}^{A\to B}(\sigma'_{AB}) := \max\left\{0, \ln\sqrt{\frac{\cosh[2s]^2}{\{\tau - m(-1+\tau)\cosh[2s]\}^2}}\right\}, \tag{29}$$

while the steerability from Bob to Alice is given by

$$\mathcal{G}^{B\to A}(\sigma'_{AB}) := \max\left\{0, \ln\sqrt{\frac{\{m(1-\tau) + \tau\cosh[2s]\}^2}{\{\tau - m(-1+\tau)\cosh[2s]\}^2}}\right\}. \tag{30}$$

The analytic derivation of these expressions is provided in Appendix B. The free space fading channel can be described by a set of pure loss channels ε_τ, represented by $\{P(\tau), \varepsilon_\tau\}$, where the loss rate τ is selected according to the probability distribution $P(\tau)$. Thus, we obtain the average quantum steerability of the quantum state [6]:

$$\mathcal{G} = \int_0^{\tau_{\max}} d\tau P(\tau)\mathcal{G}(\tau). \tag{31}$$

From Eqs. (29) and (30), it follows that the Gaussian steering depends not only on the squeezing parameter s but also on the thermal photon number and the transmittance of the free space quantum channel. The directional asymmetry of quantum steering in flat spacetime is a fundamental feature of continuous-variable quantum information theory [16,39–44]. To assess the degree of quantum steering asymmetry in free space, we define the Gaussian steerability asymmetry as

$$\mathcal{G}^{\Delta}_{AB}(\sigma'_{AB}) = |\mathcal{G}^{B\to A}(\sigma'_{AB}) - \mathcal{G}^{A\to B}(\sigma'_{AB})|. \tag{32}$$

In Figs. 2(a)–2(d), we present the Gaussian steerabilities $\mathcal{G}^{A\to B}(\sigma'_{AB})$ and $\mathcal{G}^{B\to A}(\sigma'_{AB})$ and the asymmetry $\mathcal{G}^{\Delta}_{AB}(\sigma'_{AB})$ as functions of the satellite altitude h. The initial resource is

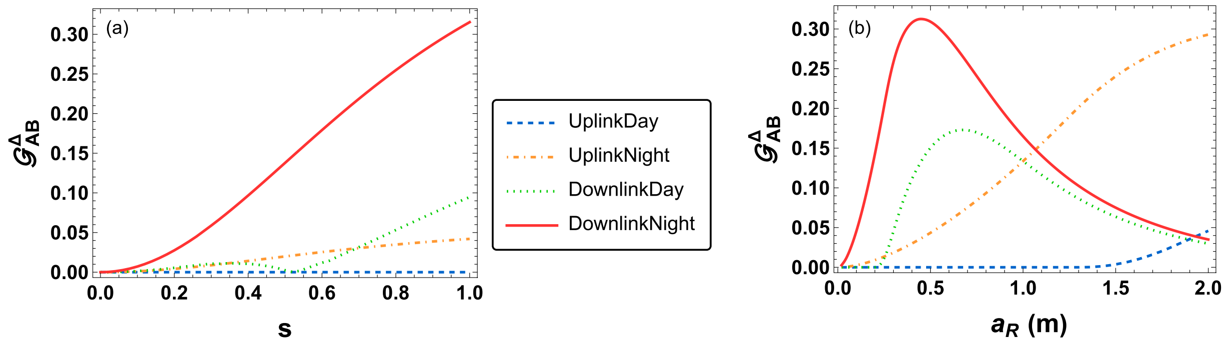

FIG. 3. The Gaussian steering asymmetry $\mathcal{G}^{\Delta}_{AB}(\sigma'_{AB})$ as functions of (a) the squeezing parameter and (b) the receiver aperture. The satellite altitude is set at $h = 300$ km.

a symmetric two-mode squeezed vacuum state, while the atmospheric channel acts on subsystem B. In the uplink configuration [Figs. 2(a) and 2(b)], the state is generated at the ground station. Alice retains one mode locally, while Bob's mode propagates upward through the atmosphere to the satellite. The monotonic decrease of steerability with altitude reflects the increasing effective loss and excess noise induced by diffraction, atmospheric attenuation, and turbulence. Under daytime conditions [Fig. 2(a)], stronger turbulence and background noise in the atmosphere significantly degrade the transmitted mode, leading to the eventual disappearance of steering. The vanishing of $\mathcal{G}^{B\to A}$ marks the transition from two-way to one-way steering, while the vanishing of $\mathcal{G}^{A\to B}$ indicates the transition from one-way steering to nonsteerability.

In the downlink configuration [Figs. 2(c) and 2(d)], the state is generated at the satellite and mode B propagates downward. Here the channel again acts on subsystem B, but the physical ordering of turbulence along the optical path differs. From the results of Figs. 2(a) and 2(c), we can see that the downlink configuration consistently achieves steerability higher than that of the uplink configuration. This discrepancy arises from the different roles of atmospheric turbulence at various stages of the optical path. In the uplink case, turbulence affects the beam at an early stage when the waist is still narrow, amplifying beam wandering and broadening over the remaining propagation distance. In contrast, in the downlink case, turbulence acts near the terminal stage of propagation, when diffraction has already expanded the beam waist. As a result, turbulence-induced wandering has a comparatively reduced impact on the received mode. Furthermore, nighttime operation yields steerability stronger than that of daytime operation due to reduced thermal background and weaker turbulence. These results demonstrate that the degradation of Gaussian steering is governed by the combined effect of channel fading and receiver-side noise, and that the observed directional asymmetry is a direct consequence of channel-induced imbalance rather than an intrinsic asymmetry of the initial state.

To further examine how the squeezing parameter and receiver configuration influence Gaussian quantum steering, we plot the Gaussian steering asymmetry $\mathcal{G}^{\Delta}_{AB}$ as a function of the receiver aperture a_R and the squeezing parameter s in Fig. 3. The maximum asymmetry occurs at $s = 1$, corresponding to the maximally entangled state, highlighting the crucial role of the initial quantum resources. For the downlink, the dependence on the receiver aperture is nonmonotonic: while increasing a_R initially improves steering by collecting more of the expanded beam, beyond a certain size, the relative impact of receiver-side thermal noise reduces the steering. Consequently, an optimal receiver aperture exists for downlink transmission, which we find to be on the order of $a_R \sim 0.4$ m under typical nighttime conditions.

V. CONCLUSIONS

We have investigated the propagation of the quantum signals in free space channels between ground stations and satellites, incorporating diffraction, atmospheric attenuation, receiver-side background photons, and turbulence into a unified fading and noisy quntum channel. We modeled the link between transmitter and receiver as an instantaneous lossy channel. Using a two-mode squeezed vacuum state, we quantified Gaussian steering and its directional asymmetry under both uplink and downlink configurations.

Our analysis shows that quantum steering degrades with increasing orbital altitude, exhibiting transitions from two-way to one-way steering and eventually to nonsteerability. Downlink transmission consistently outperforms uplink transmission because turbulence acts mainly on the expanded beam at the final stage of propagation, while in the uplink turbulence affects the initial propagation, causing stronger beam wandering. Moreover, nighttime atmospheric conditions reduce the number of background thermal photons compared to daytime, leading to improved controllability and higher transmission efficiency. Nighttime conditions, with fewer background photons, further improve steerability, making nighttime downlink the most favorable regime. These findings highlight the importance of channel asymmetries and receiver-side background photons in free space quantum communication.

A limitation of the present analysis is the focus on the zenith configuration, which corresponds to the shortest atmospheric path and provides a benchmark scenario for evaluating the combined effects of diffraction, attenuation, turbulence, and detection noise. For nonzero zenith angles, longer slant paths would generally lead to stronger cumulative channel degradation and lower steerability. Therefore, the results reported here should be understood as baseline predictions for high-elevation links. Extending this framework to arbitrary elevation angles remains an important direction for future work.

ACKNOWLEDGMENTS

This work is supported by the National Natural Science Foundation of China under Grants No. 12505084 and No. 12374408, the Natural Science Foundation of Hunan Province under Grant No. 2025JJ60019, and the Liaoning Revitalization Talents Program (Grant No. XLYC2503099).

DATA AVAILABILITY

The data that support the findings of this article are not publicly available. The data are available from the authors upon reasonable request.

APPENDIX A: DERIVATION OF THE OUTPUT COVARIANCE MATRIX

In this Appendix, we provide the detailed derivation of the covariance matrix of the bipartite Gaussian state after propagation through the free space fading and noisy quantum channel. This derivation supplements the results presented in Sec. IV and leads to Eq. (28) of the main text.

We start from the two-mode squeezed vacuum state with a covariance matrix given in Eq. (24). The covariance matrix of the initial state is [39]

$$\sigma_{AB} = \begin{pmatrix} \alpha I_2 & \beta\sigma_z \\ \beta\sigma_z & \alpha I_2 \end{pmatrix}, \tag{A1}$$

where $\alpha = \cosh(2s)$, $\beta = \sinh(2s)$, $I_2 = \mathrm{diag}(1, 1)$, and $\sigma_z = \mathrm{diag}(1, -1)$. Mode B is mixed with a thermal mode of the covariance matrix $E_T = mI_2$ through a beam splitter of transmissivity τ, represented by the symplectic transformation [6]

$$S_{B,T} = \begin{pmatrix} \sqrt{\tau} I_2 & \sqrt{1-\tau} I_2 \\ -\sqrt{1-\tau} I_2 & \sqrt{\tau} I_2 \end{pmatrix}. \tag{A2}$$

The covariance matrix of the Gaussian state describing the complete system is given by

$$\sigma'_{ABT} = [I_A \oplus S_{B,T}][\sigma_{AB} \oplus E_T] [I_A \oplus S_{B,T}]^\top. \tag{A3}$$

We derive the covariance matrix form of the complete quantum state as

$$\sigma'_{ABT} = \begin{pmatrix} I_2 & 0 & 0 \\ 0 & \sqrt{\tau} I_2 & \sqrt{1-\tau} I_2 \\ 0 & -\sqrt{1-\tau} I_2 & \sqrt{\tau} I_2 \end{pmatrix} \begin{pmatrix} \alpha I_2 & \beta\sigma_z & 0 \\ \beta\sigma_z & \alpha I_2 & 0 \\ 0 & 0 & mI_2 \end{pmatrix} \begin{pmatrix} I_2 & 0 & 0 \\ 0 & \sqrt{\tau} I_2 & \sqrt{1-\tau} I_2 \\ 0 & -\sqrt{1-\tau} I_2 & \sqrt{\tau} I_2 \end{pmatrix}^\top$$
$$= \begin{pmatrix} \alpha I_2 & \sqrt{\tau}\beta\sigma_z & (-\sqrt{1-\tau})\beta\sigma_z \\ \sqrt{\tau}\beta\sigma_z & [\tau\alpha + (1-\tau)m]I_2 & (m-\alpha)\sqrt{\tau(1-\tau)} I_2 \\ (-\sqrt{1-\tau})\beta\sigma_z & (m-\alpha)\sqrt{\tau(1-\tau)} I_2 & [(1-\tau)\alpha + \tau m]I_2 \end{pmatrix}.$$

Taking the partial trace over the thermal mode amounts to discarding the rows and columns, thus yielding the reduced bipartite covariance matrix

$$\sigma'_{AB} = \begin{pmatrix} \cosh(2s) I_2 & \sqrt{\tau}\sinh(2s)\sigma_z \\ \sqrt{\tau}\sinh(2s)\sigma_z & [\tau\cosh(2s) + (1-\tau)m]I_2 \end{pmatrix}. \tag{A4}$$

APPENDIX B: ANALYTIC EXPRESSIONS FOR GAUSSIAN STEERING

In this Appendix, we provide the explicit calculation of the Gaussian steering measures used in Sec. IV, leading to the analytic expressions reported in Eqs. (29) and (30).

For the definition of Gaussian quantum steering and the covariance matrix σ'_{AB}, one needs $\det A$, $\det B$, and $\det \sigma'_{AB}$. A represents the covariance submatrix for subsystem Alice, and B is the covariance submatrix for subsystem Bob. Using block determinant identities for 2×2 Gaussian states, a direct calculation yields

$$\det A = (\cosh[2s])^2,$$
$$\det B = \{m(1-\tau) + \tau\cosh[2s]\}^2,$$
$$\det \sigma'_{AB} = \{\tau - m(-1+\tau)\cosh[2s]\}^2, \tag{B1}$$

Employing Eq. (23), we obtain an analytic expression of the quantum steerability from Alice to Bob [10] as

$$\mathcal{G}^{A\to B}(\sigma'_{AB}) = \max\left\{0, \ln\sqrt{\frac{\cosh[2s]^2}{\{\tau - m(-1+\tau)\cosh[2s]\}^2}}\right\}, \tag{B2}$$

while the steerability from Bob to Alice is given by

$$\mathcal{G}^{B\to A}(\sigma'_{AB}) = \max\left\{0, \ln\sqrt{\frac{\{m(1-\tau) + \tau\cosh[2s]\}^2}{\{\tau - m(-1+\tau)\cosh[2s]\}^2}}\right\}. \tag{B3}$$

[1] Q. C. Sun *et al.*, Quantum teleportation with independent sources and prior entanglement distribution over a network, Nat. Photon. **10**, 671 (2016).

[2] B. Li *et al.*, Quantum state transfer over 1200 km assisted by prior distributed entanglement, Phys. Rev. Lett. **128**, 170501 (2022).

[3] J. Yin *et al.*, Satellite-based entanglement distribution over 1200 kilometers, Science **356**, 1140 (2017).

[4] D. Vasylyev, W. Vogel, and F. Moll, Satellite-mediated quantum atmospheric links, Phys. Rev. A **99**, 053830 (2019).

[5] S. Pirandola, Satellite quantum communications: Fundamental bounds and practical security, Phys. Rev. Res. **3**, 023130 (2021).

[6] T. Gonzalez-Raya, S. Pirandola, and M. Sanz, Satellite-based entanglement distribution and quantum teleportation with continuous variables, Commun. Phys. **7**, 126 (2024).

[7] S. M. Wu, H. Y. Wu, Y. X. Wang, and J. Wang, Gaussian tripartite steering in Schwarzschild black hole, Phys. Lett. B **865**, 139493 (2025).

[8] A. Einstein, B. Podolsky, and N. Rosen, Can quantum-mechanical description of physical reality be considered complete? Phys. Rev. **47**, 777 (1935).

[9] H. M. Wiseman, S. J. Jones, and A. C. Doherty, Steering, entanglement, nonlocality, and the Einstein-Podolsky-Rosen paradox, Phys. Rev. Lett. **98**, 140402 (2007).

[10] I. Kogias, A. R. Lee, S. Ragy, and G. Adesso, Quantification of Gaussian quantum steering, Phys. Rev. Lett. **114**, 060403 (2015).

[11] X. Liu, Z. Tian, and J. Jing, Entanglement dynamics in κ deformed spacetime, Sci. China Phys. Mech. Astron. **67**, 100411 (2024).

[12] P. Skrzypczyk and D. Cavalcanti, Maximal randomness generation from steering inequality violations using qudits, Phys. Rev. Lett. **120**, 260401 (2018).

[13] B. D. Jones, I. Šupić, R. Uola, N. Brunner, and P. Skrzypczyk, Network quantum steering, Phys. Rev. Lett. **127**, 170405 (2021).

[14] J. Wang, H. Cao, J. Jing, and H. Fan, Gaussian quantum steering and its asymmetry in curved spacetime, Phys. Rev. D **93**, 125011 (2016).

[15] H. Wu, X. Gong, T. Liu, and S. M. Wu, Gaussian quantum steering for continuous variables sharing in an expanding universe, Eur. Phys. J. C **84**, 856 (2024).

[16] V. Händchen, T. Eberle, S. Steinlechner, A. Samblowski, T. Franz, R. F. Werner, and R. Schnabel, Observation of one-way Einstein-Podolsky-Rosen steering, Nat. Photon. **6**, 596 (2012).

[17] Z. Qin, X. Deng, C. Tian, M. Wang, X. Su, C. Xie, and K. Peng, Manipulating the direction of Einstein-Podolsky-Rosen steering, Phys. Rev. A **95**, 052114 (2017).

[18] M. K. Olsen, Controlled asymmetry of Einstein-Podolsky-Rosen steering with an injected nondegenerate optical parametric oscillator, Phys. Rev. Lett. **119**, 160501 (2017).

[19] Y. Jiao *et al.*, Phase-selective tripartite entanglement and asymmetric Einstein-Podolsky-Rosen steering in squeezed optomechanics, Phys. Rev. A **112**, 012421 (2025).

[20] X. Huang, X. Jiang, Y. Wang, S. Liu, Z. Wang, and S. Wu, Can boundary configuration be tuned to optimize directional quantum steering harvesting? J. High Energy Phys. 09 (2025) 023.

[21] R. L. Fante, Electromagnetic beam propagation in turbulent media, Proc. IEEE **63**, 1669 (1975).

[22] R. L. Fante, Electromagnetic beam propagation in turbulent media: An update, Proc. IEEE **68**, 1424 (1980).

[23] D. Vasylyev, A. Semenov, and W. Vogel, Atmospheric quantum channels with weak and strong turbulence, Phys. Rev. Lett. **117**, 090501 (2016).

[24] D. Vasylyev, A. Semenov, and W. Vogel, Toward global quantum communication: Beam wandering preserves nonclassicality, Phys. Rev. Lett. **108**, 220501 (2012).

[25] S. Pirandola, Limits and security of free-space quantum communications, Phys. Rev. Res. **3**, 013279 (2021).

[26] M. Ghalaii and S. Pirandola, Continuous-variable measurement-device-independent quantum key distribution in free-space channels, Phys. Rev. A **108**, 042621 (2023).

[27] V. Giovannetti, S. Guha, S. Lloyd, L. Maccone, and J. H. Shapiro, Minimum output entropy of bosonic channels: A conjecture, Phys. Rev. A **70**, 032315 (2004).

[28] G. Adesso and F. Illuminati, Entanglement in continuous variable systems: Recent advances and current perspectives, J. Phys. A: Math. Theor. **40**, 7821 (2007).

[29] D. E. Bruschi, A. Datta, R. Ursin, T. C. Ralph, and I. Fuentes, Quantum estimation of the Schwarzschild spacetime parameters of the Earth, Phys. Rev. D **90**, 124001 (2014).

[30] Q. Liu, C. Wen, Z. Tian, J. Jing, and J. Wang, Gravity-enhanced quantum spatial target detection, Phys. Rev. A **105**, 062428 (2022).

[31] O. Svelto, *Principles of Lasers* (Springer, Berlin, 2010).

[32] E.-L. Miao, Z.-F. Han, S.-S Gong, T. Zhang, D.-S. Diao, and G.-C. Guo, Background noise of satellite-to-ground quantum key distribution, New J. Phys. **7**, 215 (2005).

[33] C. Bonato, A. Tomaello, V. Da Deppo, G. Naletto, and P. Villoresi, Feasibility of satellite quantum key distribution, New J. Phys. **11**, 045017 (2009).

[34] R. E. Hufnagel and N. R. Stanley, Modulation transfer function associated with image transmission through turbulent media, J. Opt. Soc. Am. **54**, 52 (1964).

[35] G. C. Valley, Isoplanatic degradation of tilt correction and short-term imaging systems, Appl. Opt. **19**, 574 (1980).

[36] H. T. Yura, Short-term average optical-beam spread in a turbulent medium, J. Opt. Soc. Am. **63**, 567 (1973).

[37] C. Weedbrook, S. Pirandola, R. García-Patrón, N. Cerf, T. Ralph, J. Shapiro, and S. Lloyd, Gaussian quantum information, Rev. Mod. Phys. **84**, 621 (2012).

[38] G. Adesso, D. Girolami, and A. Serafini, Measuring Gaussian quantum information and correlations using the Renyi entropy of order 2, Phys. Rev. Lett. **109**, 190502 (2012).

[39] G. Adesso, I. Fuentes-Schuller, and M. Ericsson, Continuous-variable entanglement sharing in noninertial frames, Phys. Rev. A **76**, 062112 (2007).

[40] S. Wollmann, N. Walk, A. J. Bennet, H. M. Wiseman, and G. J. Pryde, Observation of genuine one-way Einstein-Podolsky-Rosen steering, Phys. Rev. Lett. **116**, 160403 (2016).

[41] K. Sun *et al.*, Experimental quantification of asymmetric Einstein-Podolsky-Rosen steering, Phys. Rev. Lett. **116**, 160404 (2016).

[42] W. Liu, C. Wen, and J. Wang, Lorentz violation alleviates gravitationally induced entanglement degradation, J. High Energy Phys. 01 (2025) 184.

[43] X. Liu, C. Zeng, and J. Wang, Generation of quantum entanglement in superposed diamond spacetime, Eur. Phys. J. C **85**, 539 (2025).

[44] I. Fuentes-Schuller and R. B. Mann, Alice falls into a black hole: Entanglement in non-inertial frames, Phys. Rev. Lett. **95**, 120404 (2005).